Newcastle University

MAS8019 project

Gravitational Waves from the Big Bang

2014/2015

Written by:
David Matthias

Supervisor:
Prof. Ian Moss

Abstract

This project will focus on the role that primordial gravitational waves from the big bang have in modern cosmology. It will begin by defining these fundamental waves, where they are located and what experiments have been put in place to detect them. It will then include the theory of inflation, and how various potential energies can be manipulated to result in graphical plots of gravitational wave fluctuations against frequency density. Then two models will be considered, using MATLAB to produce the plots required.

Contents

Chapter 1

Introduction

This section provides information about gravitational waves, the cosmic microwave background, polarisation into E-modes and B-modes, and the claim of detection from 2014.

1.1 Gravitational Waves

In 1916, Albert Einstein produced a paper entitled “Nherungsweise Integration der Feldgleichungen der Graviation”, (“Approximate integration of the field equations of gravitation” in English), in which he predicted the existence of gravitational waves [1]. This prediction was based on his theory of general relativity, in which gravitation is explained via the spacetime curvature [2]. The effect that the curved spacetime has on objects is more commonly recognised as gravity [2].

So what exactly is a gravitational wave? When a big object moves, the spacetime curvature must adjust as to follow the position of the object, resulting in a delayed reaction time for spacetime to change; this is due to nothing being able to travel faster than the speed of light [2]. This results in a ripple effect within the spacetime itself, defined as gravitational waves [2].

The main problem with studying these waves is detecting them in the first place, as attempts so far have proven unsuccessful, but they are still an important area of study as they provide an exclusive insight into many intense systems, such as the big bang [2].

This project will focus on primordial gravitational waves, i.e. ones that are within the cosmic microwave background which were produced by the big bang [2, 3].

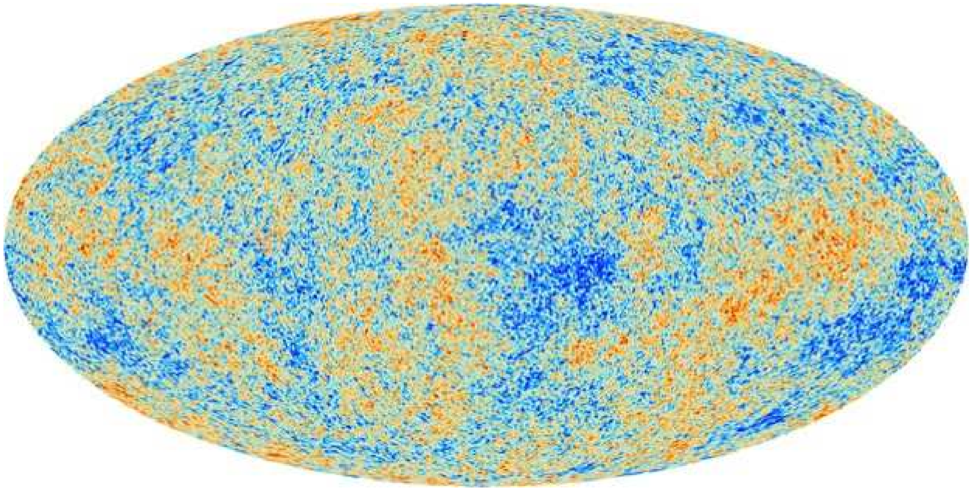

Figure 1.1: A mapping of the anisotropies in the entire CMB as performed by the Planck satellite. Taken from the European Space Agency's website [5].

1.2 Cosmic Microwave Background

The cosmic microwave background (CMB) is radiation which is the "afterglow" of the big bang [2], which was discovered accidentally by two radio-astronomers in 1964 [4]. Since its discovery, the CMB has been heavily studied, as it is thought to be the most convincing piece of evidence for the big bang theory, as it preserves a picture of the early universe and could hold the key to unlocking the initial conditions [5].

Unfortunately, measurements from earth face the problem of interference, resulting in less accurate measurements. This is where the Planck satellite comes in. On the 14th of May 2009, the Planck satellite was launched with the primary objective to map the CMB; it did this by rotating on an axis and measuring via strips to complete a full mapping [5]. Figure 1.1 shows the completed CMB as surveyed by Planck [5]. It is possible to see the uneven temperature distribution in the CMB, i.e. the anisotropies which are caused by the effects of gravitational waves.

This is acknowledged as the definitive picture of the CMB, as Planck was operated with an accuracy which was governed by fundamental limits [5]. Due to background noise, the limit of certainty Planck reached is the natural limit of measurement accuracy, making its measurement of the temperature variations the most accurate they will ever be [5].

The Planck satellite also performed many measurements of the temperature fluctuations as well as mapping them. Figure 1.2 shows a graph of

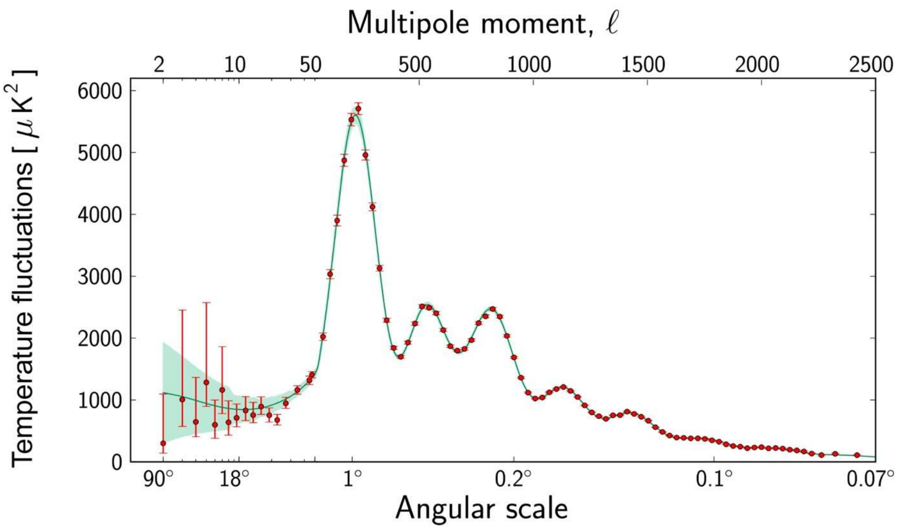

Figure 1.2: Observations of the temperature fluctuations in the CMB at different angular scales as measured by Planck. The red dots are each individual measurement, presented with error bars. The green curve represents the 'standard model of cosmology'. The pale green area represents all variations of this model which comply with the Planck data. Taken from the European Space Agency's website [5].

these measurements at different angular scales, from largest on the left to smallest on the right, against the temperature fluctuations [5]. These temperature fluctuations involve a term $C(l)$, which represent Laplace's spherical harmonics. Each red dot is a measurement taken by Planck, with error bars corresponding to errors in the actual measurement itself, and due to the uncertainty that arises from there being only a few points in the sky that measurements can be taken; this second uncertainty factor becomes more prominent at the larger angular scales, as seen with the larger error bars to the left of the plot [5]. The green curve corresponds to the 'standard model of cosmology' which fits the Planck data the best, with the pale green area to the left of the plot corresponding to all variations of this model which comply with the Planck data [5].

At the smaller angular scales, the Planck measurements agree with the predictions of the standard model, but as the angular scales get larger than six degrees, the points deviate from the main green curve, and even one point lies outside of the green area, implying that the standard model of cosmology

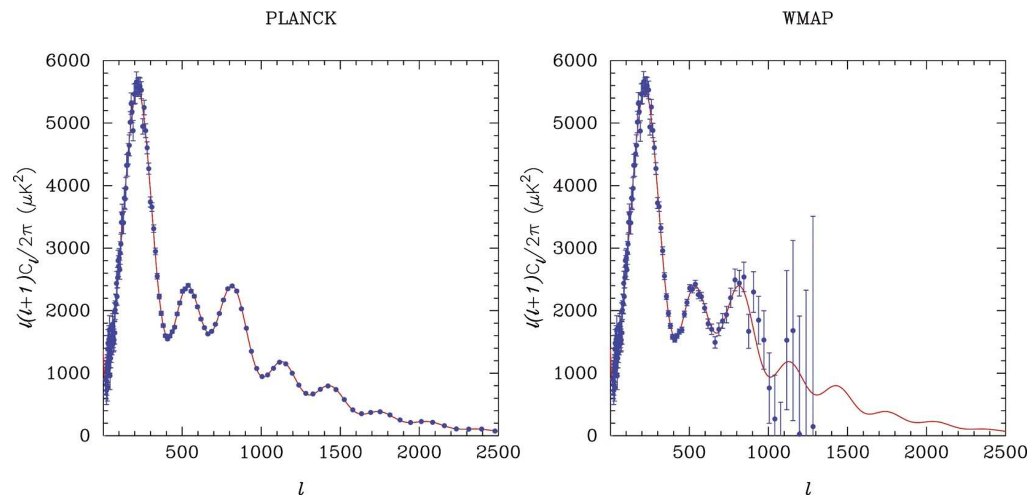

Figure 1.3: A direct comparison of the measurements of the temperature fluctuations in the CMB as measured by Planck (left) and WMAP (right). Due to the smaller error bars and ability to plot more points as the angular scale gets smaller, the Planck satellite is seen as the more accurate of the two. Taken from the European Space Agency's website [5].

might have some areas which need to be reassessed [5].

To show how accurate the measurements of the Planck satellite are, they can be compared to the analysis of another mission to measure the CMB fluctuations. The Wilkinson Microwave Anisotropy Probe (WMAP) was launched in 2001, and it produced the first mapping of the CMB fluctuations to a resolution of 0.2 degrees on the angular scale [6].

Figure 1.3 shows a direct comparison of the observations of the Planck satellite and the WMAP [5]. As the angular scales get smaller, not only do the points start to leave the main curve, the error bars for the WMAP readings become much larger than Planck's. Planck was also able to get readings of much smaller angular scales than the WMAP, resulting in a significant improvement; this was due to the increased angular resolution and sensitivity of instruments which the Planck satellite had [5].

1.3 Claim of Detection

The way that gravitational waves could be detected in the CMB would be to look at the polarisation patterns, as tiny fluctuations in the spacetime, due to the rapid expansion of the big bang, could have produced a background of gravitational waves that could still exist today [2].

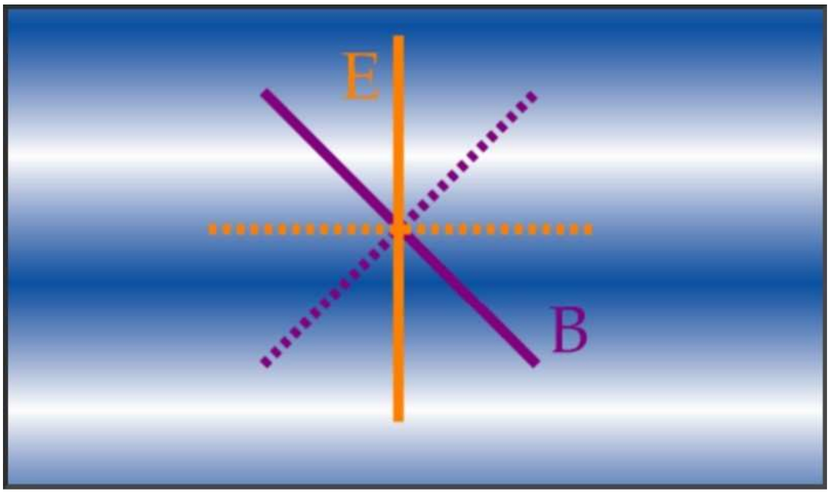

Figure 1.4: A visual example of the E-mode and B-mode polarisation angles superimposed onto a plane wave travelling in the up-down direction. The E-mode polarisations are parallel and perpendicular to the direction of the wave. The B-mode polarisations are at forty-five degree angles to the direction of the wave. Taken from the B-modes section on Professor Wayne Hu's webpage [7].

Polarisation patterns separate geometrically into two cases, E-modes and B-modes [7]. If a plane wave is travelling in the up-down direction, it can be polarised in a number of different directions; if the polarisation is parallel or perpendicular to the wave's original direction it is called an E-mode polarisation, and if the polarisation occurs at a forty-five degree angle to the wave's original direction it is called a B-mode polarisation [7]. Figure 1.4 shows a visual representation this [7].

The reason this is important, is because density perturbations can only have a parallel polarisation, resulting in exclusively E-mode polarisation, whereas gravitational waves can generate both polarisation patterns, meaning that they have an element of B-mode polarisation [7]. Detection of B-modes is a current hot-topic in cosmology, as their discovery implies gravitational waves, which in turn provides experimental evidence for inflation and the big bang.

The BICEP2 (Background Imaging of Cosmic Extragalactic Polarisation) telescope is located in the South Pole. Its main objective was to locate the B-modes located in the CMB [8]. In March 2014, the BICEP2 collaboration published a paper, stating that they had detected B-modes created by the gravitational waves; these results produced the value for the tensor-scalar ratio (see section 2.6) as 0.2 with a confidence region of $+0.07$ and -0.05, which rejected the null hypothesis of the tensor-scalar ratio being equal to zero [8].

However, in a revised edition of their paper which was submitted in June 2014, the BICEP2 collaboration added that there was lowered confidence in these findings as there was a chance that the signal could have been caused by a cosmological dust signal [8]. A joint analysis between the Planck and BICEP2 data sets further concluded that the signal detected and the strength of the dust signal was the same magnitude [9]. This led to the conclusion that no matter how 'clean' an area of the sky is, the dust signal needs to be examined [9].

All of these efforts to detect gravitational waves have not been in vain. Although the gravitational waves have not yet been detected, due to a more complete understanding of the dust signal, there are now extremely accurate predictions of what signals the waves will produce [9], hopefully making detection easier in the near future.

Chapter 2

Inflation

This section focuses on the theory of inflation, starting with a brief history and then going on to the crucial equations which define this method. It will then finish with a worked example, showing all these equations in action, resulting in a plot of gravitational wave fluctuations against frequency density.

2.1 What is Inflation?

Prior to investigating gravitational waves further, it is necessary to review the theory of inflation. The standard big bang model needs initial conditions; unfortunately there are two things which make these conditions complicated to explain. These are the horizon problem - the early universe is assumed to be homogeneous even though separate regions were causally disconnected - and the flatness problem - the initial value of the Hubble constant needs to be chosen extremely precisely to be able to model the universe as flat as what has been observed [10].

In 1981, Alan Guth provided the inflationary hypothesis in order to create a scenario which avoided the horizon and flatness problems [10], and which would help to explain the initial conditions for the big bang, as what triggered inflation is still unknown. Figure 2.1 shows a visual example of the inflationary model compared with the standard model.

In cosmological terms, inflation is defined as an era just after the big bang when the universe expanded exponentially in an extremely small time frame. As seen from Figure 2.1, this period is thought to have occurred 10^{-35} seconds after the big bang. During this extremely small time period, it is thought that the size of the universe increased by a scale factor of around 10^{26} [6]. After this time period, the universe continued to expand but at a

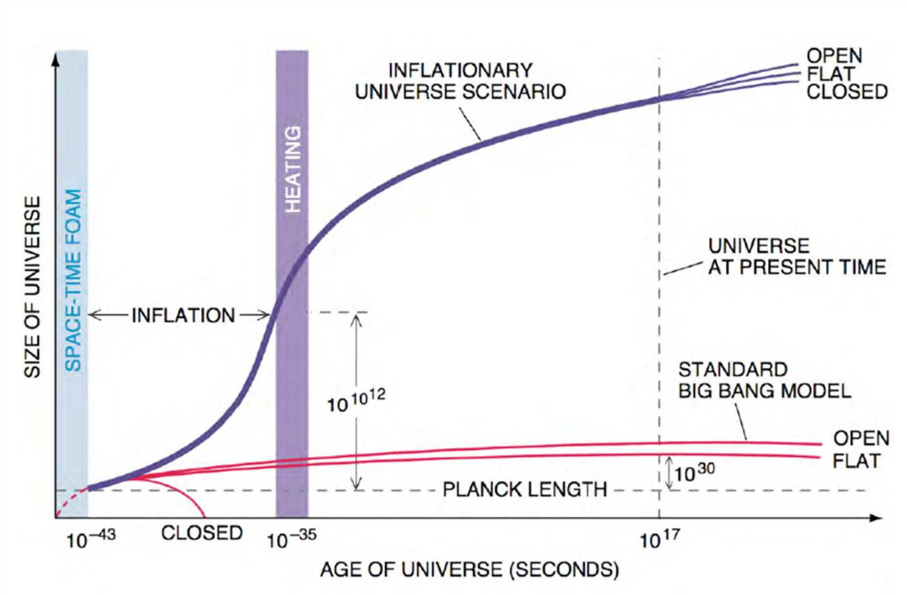

Figure 2.1: Graph showing the size of the universe against the time in seconds measured after the big bang. This plot shows the inflationary universe scenario compared with the standard big bang model. Taken from a lecture by Andrei Linde in 2007, found at "http://www.mpa-garching.mpg.de/lectures/Biermann_07/LindeLecturesMunich1.pdf".

slower rate.

Since its inception, the theory has been extremely influential, and is widely accepted as the favoured contender for the origin of structure in the universe [11].

2.2 Equations of Motion

The theory of inflation includes many equations which include a term for potential energy, making it possible to interpret results for various potential energy models. But first, it is necessary to look at the equations of motion that define the universe. The properties of the materials contained inside the universe control the expansion [11]; these are usually specified as the energy density $\rho(t)$ and the pressure $p(t)$ (which are both functions of time). These quantities are often related by an equation of state, i.e.

$$p(t) \equiv \rho(t) \ .$$

There are two equations which describe how the universe expands. These are the Friedmann equation, given by

$$3\left(\frac{\dot{a}^2}{a^2}+\frac{k}{a^2}\right)=8\pi G\rho \ , \tag{2.1}$$

and the fluid equation which is given by

$$a\dot{\rho}+3\dot{a}\left(\rho+\frac{p}{c^2}\right)=0 \ , \tag{2.2}$$

where a is the scale factor of the universe, k is a constant known as the spatial curvature, G is the gravitational constant, c is the speed of light, and the dots above the variables represent the time derivatives [11].

Equations (2.1) and (2.2) can be combined to form a new acceleration equation, written as

$$\ddot{a}=-\frac{4}{3}\pi G\left(\rho+\frac{3p}{c^2}\right)a \ ,$$

which does not have k appearing [11].

The spatial curvature k is usually scaled to either -1, $+1$ or 0, representing open, closed and flat universes respectively [11]. As it is preferred that the universe is flat, from now on k shall be set to equal zero. Also, it is common cosmological practice to choose limits in which the speed of light, c, is set equal to one; note that this makes the energy and mass densities interchangeable as now $p/c^2 = p$ [11]. This results in equation (2.1) becoming

$$3H^2=8\pi G\rho \ , \tag{2.3}$$

where

$$H=\frac{\dot{a}}{a} \ , \tag{2.4}$$

is defined as the Hubble Parameter. Similarly, equation (2.2) becomes

$$a\dot{\rho}+3\dot{a}\left(\rho+p\right)=0 \ . \tag{2.5}$$

For a homogeneous scalar field, the field is a function of time alone. A potential energy can be defined as $V(\phi)$, which includes the scalar field. The mass density and the pressure can now be defined as

$$\rho=\frac{1}{2}\dot{\phi}^2+V(\phi) \ , \tag{2.6}$$

and

$$p=\frac{1}{2}\dot{\phi}^2-V(\phi) \ , \tag{2.7}$$

where, in both equations, the first term can be thought of as kinetic energy, and the second as potential energy. [11]. These equations can be substituted into the equations of motion to obtain a new set of equations containing the homogeneous scalar field. Substituting equations (2.6) and (2.7) into equation (2.3) gives

$$3H^2 = 8\pi G\left(V\left(\phi\right) + \frac{1}{2}\dot{\phi}^2\right) \ , \tag{2.8}$$

and substituting equations (2.6) and (2.7) into equation (2.5) gives

$$\ddot{\phi} + 3H\dot{\phi} + \frac{\partial V}{\partial \phi} = 0 \ . \tag{2.9}$$

2.3 The Slow-Roll Approximation

Now the equations of motion containing a scalar field have been defined, they can be solved. The standard practice to do this is a method called the slow-roll approximation. It assumes that the potential is flat enough that the scalar field would roll slowly towards a minimum, at which inflation would end [11]. A visual example of this is shown in Figure 2.2, where the ball represents the potential slowly rolling downwards.

The slow-roll approximation involves neglecting a term in each equation, resulting in simpler expressions [11]. Ignoring $\dot{\phi}$ in equation (2.8) yields

$$3H^2 = 8\pi GV \ , \tag{2.10}$$

and ignoring $\ddot{\phi}$ in equation (2.9) yields

$$3H\dot{\phi} + \frac{\partial V}{\partial \phi} = 0 \ . \tag{2.11}$$

Slow roll parameters can be introduced as [12]

$$\epsilon\left(\phi\right) = \frac{1}{16\pi G}\left(\frac{1}{V}\frac{\partial V}{\partial \phi}\right)^2 \ , \tag{2.12}$$

and

$$\eta\left(\phi\right) = \frac{1}{8\pi G}\frac{1}{V}\left(\frac{\partial^2 V}{\partial \phi^2}\right) \ , \tag{2.13}$$

where the ϵ measures the slope of the potential and η measures the curvature [11]. Almost all results of equations can be expressed in terms of these two parameters, for example

$$\frac{\ddot{\phi}}{H\dot{\phi}} = \epsilon - \eta \ , \tag{2.14}$$

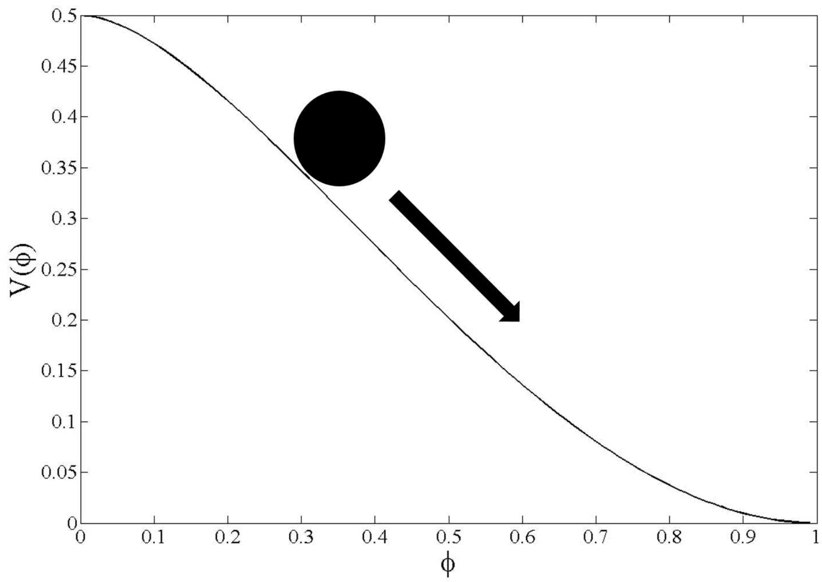

Figure 2.2: Visual example of a slow-roll potential. The potential used is the soft SUSY model (see section 3.3). Think of the ball as the potential, slowly rolling towards the minimum, hence the name 'Slow-Roll'.

and

$$\frac{\dot{H}}{H^2} = -\epsilon \ , \tag{2.15}$$

are two equations which will be used to derive later results.

2.4 Amount of Inflation

The slow-roll approximation is based on the idea that at some point inflation will end. So under what conditions will this happen? Inflation is defined as an acceleration, so, inflation will end when the acceleration is equal to zero, as at this point the universe will no longer be expanding i.e. accelerating outwards. As the equation for the Hubble Parameter contains a term for velocity ($\dot{a}$), it seems logical to start by manipulating equation (2.4) to give

$$\dot{a} = aH \ .$$

Differentiating this gives a term for acceleration on the left hand side, resulting in the equation

$$\ddot{a} = \dot{a}H + a\dot{H} \ .$$

Using equation (2.15) and the rearranged Hubble parameter, the above expression can be rewritten as

$$\ddot{a} = aH^2 - aH^2\epsilon \ .$$

By noting the common factor of aH^2, this can be expressed as

$$\ddot{a} = aH^2 \left(1 - \epsilon\right) \ .$$

As a and H are positive constants, it can be inferred that inflation ends when ϵ is equal to one, as this term reduces the right hand side of the above equation to zero.

It is also possible to calculate the amount of inflation that takes place between a measured point in time and the end of inflation. If $t_\star$ is denoted to be the time which a measurement takes place and t_f is denoted to be the time at the end of inflation, it can be written that

$$N = \ln\left(\frac{a\left(t_f\right)}{a\left(t_\star\right)}\right) \ ,$$

where N is called the number of e-folding's, as the amount of inflation is stated to be the log of the amount of expansion [11]. It is possible to show that the above equation can be written as

$$N = -8\pi G \int_{\phi_\star}^{\phi_f} \frac{V}{V_\phi} d\phi \ . \tag{2.16}$$

The derivation of this is given in appendix A.1. As it has been seen that inflation ends when ϵ is equal to one, it can be used to find the value for ϕ_f in the integral. For simple potentials, N can be written in terms of slow roll parameters.

The number of e-folds is believed to lie between fifty and sixty [13], so the majority of plots that involve this term have two points joined by a line, one where N is set equal to fifty, and one where N is set equal to sixty.

2.5 Primordial Power Spectrums

Primordial fluctuations in the universe are described by power spectrums [14]. There are two main types; the power spectrum for scalar fluctuations, i.e. the mean square density fluctuation amplitude $\delta\rho/\rho$, and the power spectrum for tensor fluctuations, i.e. the mean square of the gravitational wave amplitude [14]. These equations are both evaluated when the co-moving wavenumber, k, is equal to the horizon size, aH [14]. This is known as the horizon crossing, i.e. when a mode crosses the horizon [14]. The power spectrum for the scalar is given by

$$\mathcal{P}_S = \frac{1}{4\pi^2}\frac{H^4}{\dot{\phi}^2} \ , \tag{2.17}$$

and the power spectrum for the tensor is given by

$$\mathcal{P}_T = \frac{2}{\pi^2}\frac{H^2}{M_p^2} \ , \tag{2.18}$$

where M_p^2 is a constant with the value $(8\pi G)^{-1}$ [14]. Both of these equations are formulated via a Fourier transform.

2.6 Tensor-Scalar Ratio and Spectral Index

The tensor-scalar ratio, r, is defined as the ratio between the power spectrum for the tensor $\mathcal{P}_T$ and the power spectrum for the scalar $\mathcal{P}_S$, i.e.

$$r = \frac{\mathcal{P}_T}{\mathcal{P}_S} \ .$$

It is possible to show that the above equation can be written as

$$r = 16\epsilon \ . \tag{2.19}$$

The derivation of this is given in appendix A.2. This is the equation for the tensor-scalar ratio in terms of slow roll parameters. As r is the ratio between the mean square of the gravitational wave amplitude and the mean square density fluctuation amplitude, it is the term that directly involves gravitational waves.

The expression for the power spectrum for the scalar fluctuations, $\mathcal{P}_S$, can also be defined as a power law, which includes the scalar spectral index, n_S; this is given by

$$\mathcal{P}_S \approx Ak^{n_S-1} \ ,$$

where A is a constant and k is the co-moving wavenumber [14]. It is possible to show that the above equation can be re-evaluated in terms of n_S, resulting in the equation

$$n_s = 1 + 2\eta - 6\epsilon + \mathcal{O}\left(\epsilon\right) \ . \tag{2.20}$$

The derivation of this is given in appendix A.3. This is the equation for the spectral index in terms of slow roll parameters.

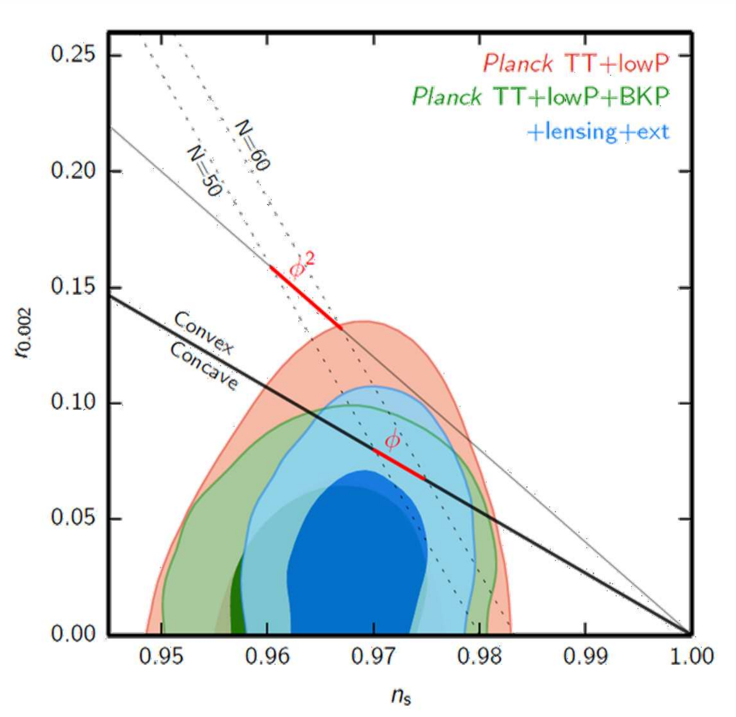

Figure 2.3: Plots of the tensor-scalar ratio on the y-axis against the spectral index on the x-axis for potentials of ϕ and ϕ^2. The dotted lines show where N is equal to fifty and sixty for both potentials. Different coloured areas represent the different data sets used, as labelled in the top right. The darker areas show the 95% confidence regions, and the lighter areas show the 68% confidence regions. Taken from the Planck 2015 XIII Cosmological Parameters paper [15].

As these are observable parameters [14], the tensor-scalar ratio and the spectral index can be plotted against each other. Figure 2.3 shows plots of the tensor-scalar ratio against the spectral index for two different types of potential, where the darker area is the 95% confidence interval, the lighter area is the 68% confidence interval, 'TT' is the best fit for the Planck CMB temperature power spectrum, 'lowP' is the use of polarisation information from the Planck temperature and polarisation pixel-based likelihood, 'BKP' is the default configuration of the BICEP2/Keck Array and Planck likelihood, 'lensing' is the Planck lensing likelihood and 'ext' is external data [15].

As gravitational waves have not been observed yet, the null hypothesis is to have r set equal to zero. This is why the 68% and 95% confidence regions are centred around r equal to zero.

2.7 A Worked Example

To show these equations in action a potential needs to be specified. To keep things simple, the potential will be defined as

$$V = \frac{1}{4}\lambda\phi^4 \ .$$

Substituting into equation (2.12) yields

$$\begin{aligned}\epsilon &= \frac{1}{16\pi G}\left(\frac{4}{\lambda\phi^4}\lambda\phi^3\right)^2 \ , \\ &= \frac{1}{\pi G\phi^2} \ .\end{aligned}$$

Similarly, substituting into equation (2.13) yields

$$\begin{aligned}\eta &= \frac{1}{8\pi G}\frac{4}{\lambda\phi^4}3\lambda\phi^2 \ , \\ &= \frac{3}{2}\frac{1}{\pi G\phi^2} \ , \\ &= \frac{3}{2}\epsilon \ .\end{aligned}$$

Now, substituting into equation (2.16) yields

$$\begin{aligned}N &= -2\pi G\int_{\phi_\star}^{\phi_f}\phi \ d\phi \ , \\ &= -\pi G\left[\phi^2\right]_{\phi_\star}^{\phi_f} \ , \\ &= -\pi G\phi_f^2 + \pi G\phi_\star^2 \ .\end{aligned}$$

It can be written that

$$\begin{aligned}N &= \frac{1}{\epsilon\left(\phi_\star\right)} - \frac{1}{\epsilon\left(\phi_f\right)} \ , \\ &= \frac{1}{\epsilon} - 1 \ ,\end{aligned}$$

as $\epsilon\left(\phi_f\right)$ is the value of ϵ at the end of inflation, which is equal to one.

Now that equations have been defined , ϵ and η can be expressed in terms of N. Rearranging the above expression yields

$$\epsilon = \frac{1}{N+1} \ .$$

Now ϵ being equal to one implies that $\eta(\pi_f) = 3/2$. Also $\eta = 3/2\epsilon$ implies that $\epsilon = 2/3\eta$, so

$$N = \frac{3}{2\eta} - \frac{2}{3} \ .$$

Rearranging the above expression yields

$$\eta = \left(\frac{9}{6N+4}\right) \ .$$

Now that the slow-roll parameters are expressed in terms of N, it is possible to substitute these into the equations for the tensor-scalar ratio and spectral index. Using equation (2.19) yields

$$\begin{aligned} r &= 16\epsilon \ , \\ &= \frac{16}{N+1} \ . \end{aligned}$$

Similarly, using equation (2.20) yields

$$\begin{aligned} n_S &\approx 1 + 2\eta - 6\epsilon \ , \\ &= 1 + 2\left(\frac{9}{6N+4}\right) - 6\left(\frac{1}{N+1}\right) \ , \\ &= 1 + \frac{9}{3N+2} - \frac{6}{N+1} \ . \end{aligned}$$

From before, N is usually believed to be between 50 and 60, so specific values for the tensor-scalar ratio and the spectral index can be found for these two separate values. When N is fifty

$$r \approx 0.314 \ , \ \ n_S \approx 0.942 \ .$$

Similarly, when N is sixty

$$r \approx 0.262 \ , \ \ n_S \approx 0.951 \ .$$

It is possible to plot these points on the graph of r vs. n_S. Before plotting, it is better to rescale ϕ to equal x/M_p^2, which allows λ to drop out, making it easier to plot. This results in the graph shown in Figure 2.4. The MATLAB code for this plot is given in appendix B.1.

The graph has been edited to incorporate the Planck data, and to show explicitly the values where N is equal to fifty and sixty. When comparing, it is clear to see that the line is nowhere near the 95% or 68% confidence regions, therefore it can be deduced that this is not a good model when comparing with the Planck data.

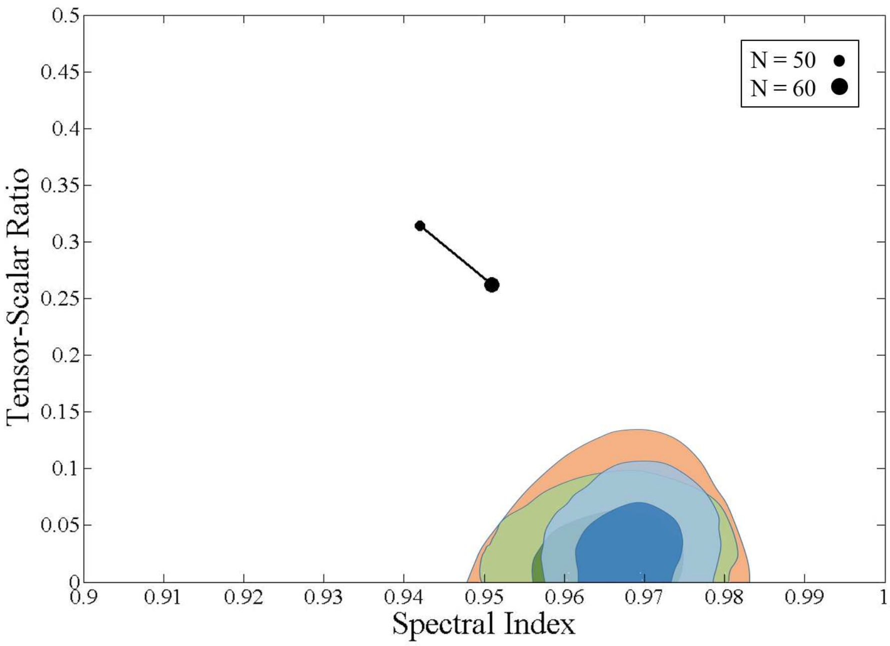

Figure 2.4: Plot of tensor-scalar ratio against spectral index for the potential $V = 1/4\lambda\phi^4$. The confidence regions of 68% and 95% from the Planck data have been superimposed. The labelling of the points where N is equal to fifty and sixty has been given in the top right of the plot.

Chapter 3

Using MATLAB

This section introduces the need for programming due to complicated potentials, as well as two examples, one of which is a model that is 'new' in the sense that it has not been studied in the Planck data release. Both result in the style of plot as seen in section 2.7.

3.1 Why MATLAB?

Theoretically, any potential can be used to get a tensor-scalar ratio vs. spectral index plot. The worked example in section 2.7 shows how relatively simple potentials can be put through the equations of inflation, which in turn result in numbers to be able to plot on a graph. However, due to the equation for N being an integral, more complex potentials can be extremely hard to solve analytically. Therefore MATLAB is required.

MATLAB is an incredibly powerful computing software that is extremely helpful when it comes to evaluating complicating integrals. It also has a powerful plotting tool which has proved advantageous when it comes to creating graphs for the potentials described in this section.

3.2 Starting simple

To be able to check if the code that has been created is working, it is best to start with a simple potential model that can also be solved analytically as to be able to check the output. A suitable potential for this purpose is

$$V = \frac{1}{4}\lambda\left(\phi_0^4 - \phi^4\right) \ . \tag{3.1}$$

Before any sort of computing, it is much simpler in the long run if the potential is scaled in term of x to get rid of any unwanted constants. It is advantageous to use the substitution

$$\phi = \frac{x}{x_0} \ . \tag{3.2}$$

This results in equation (3.1) becoming

$$V = 1 - \frac{x^4}{x_0^4} \ . \tag{3.3}$$

This is much simpler to work with in MATLAB. Note how the λ and $1/4$ can be dropped as they would get cancelled out when calculating ϵ and η.

There are two things that need to be done by hand; the derivative and the double derivative. Differentiating equation (3.3) gives

$$V' = -4\left(\frac{x^3}{x_0^4}\right) \ , \tag{3.4}$$

and then in turn, differentiating equation (3.4) results in

$$V'' = -12\left(\frac{x^2}{x_0^4}\right) \ . \tag{3.5}$$

Now that these have been evaluated, it is time to formulate the code. Firstly, parameters and equations need to be defined by inputting our equations like so

```
x0 = 10.0;
v = @(x) 1 - (x.^4)/(x0.^4);
dv = @(x)  -4*(x.^3)/(x0.^4);
d2v = @(x)  -12*(x.^2)/(x0.^4);
eps = @(x) 0.5*((dv(x)).^2)./((v(x)).^2);
eta = @(x) (d2v(x))./v(x);
```

Therefore the potential, derivatives and slow-roll parameters have been input into MATLAB. Here, the value for x_0 has been given as ten, but at this stage it does not matter too much. The M_p^2 has been omitted as the substitution earlier means that the calculation of ϵ and η would have resulted in it disappearing.

To see what the graph of this potential looks like, the following commands can be input into MATLAB

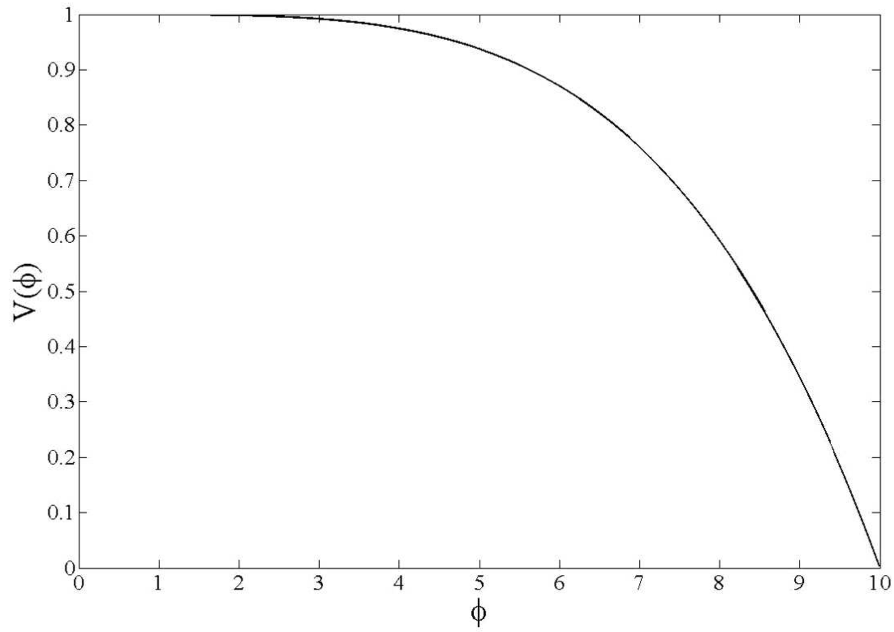

Figure 3.1: Graph of $V(\phi)$ against ϕ for the model $V = (1/4)\lambda\left(\phi_0^4 - \phi^4\right)$. Here, x_0 has been taken to be ten.

```
x = 1.0e-6:0.01:x0-1.0e-6;
y = v(x);
figure
plot(x,y)
```

which results in the graph seen in Figure 3.1. This shows that using the slow-roll approximation is suitable as the potential slowly rolls to a minimum. As the graph has a sheer drop off, it can also be inferred that this potential will tend to a linear potential when x_0 is large. For the amount of inflation, as seen before, it is necessary to find when ϵ is equal to one. For this, MATLAB has an inbuilt function, called fzero, to find when an equation is equal to zero in a certain range. Setting up the following MATLAB code is sufficient

```
eps1 = @(x) eps(x)-1.0;
xr = [1.0e-6,x0-1.0e-6];
xf = fzero(eps1,xr);
```

as this will return the required result. Note the ϵ_1 term subtracts one off ϵ, so when ϵ is equal to one, ϵ_1 will be equal to zero. The range x_r is used due to the potential having a term where x_0 is on the denominator, so x_0 cannot be equal to zero, but setting up the range as shown above bypasses this as it can take a value extremely close to zero and not return an error. Finally, the x_f term uses the fzero function, so this term will be the value of the potential when ϵ equals zero, i.e. when inflation ends.

It is now possible to set up the integral for the number of e-folds, using the following code

```
xstar = 4.1357;
efolds = @(x) v(x)./dv(x);
N = -integral(efolds,xstar,xf)
```

which results in a value for N for a choice of x_0 and $x_\star$. In this case, the $x_\star$ is a value inputted and changed to find N equal to fifty and sixty by trial and error. The e-folds term sets up the integral, and N uses MATLAB's inbuilt integral function to evaluate the value. As the potential has a negative gradient, the limits on the integration have been swapped, and the negative value of this is taken to return a positive value for N. By using trial and error, N is roughly found to be equal to fifty when $x_\star$ is equal to 4.136, and N is roughly found to be equal to sixty when $x_\star$ is equal to 3.873, with both values for $x_\star$ given to four significant figures.

For a single value of $x_\star$, the tensor-scalar ratio and spectral index can be calculated by setting up the equations like so

```
r = 16.*eps(xstar);
n = 1 + 2*eta(xstar) - 6*eps(xstar);
```

and once these values have been calculated, they can be plotted against each other using

```
plot(n,r,'k')
```

however, this just results in the one point being plotted for a singular $x_\star$.

To create a line, much like the one seen in the worked example earlier, a for loop can be created which runs multiple values for $x_\star$, calculating the tensor-scalar ratio for each one, then plotting on a graph. This for loop takes the form

```
for i = 3.8728:0.0010516:4.1357
    xstar = i;
    r = 16.*eps(xstar);
    n = 1 + 2*eta(xstar) - 6*eps(xstar);
    plot(n,r,'k')
    xlim([0.94 1])
```

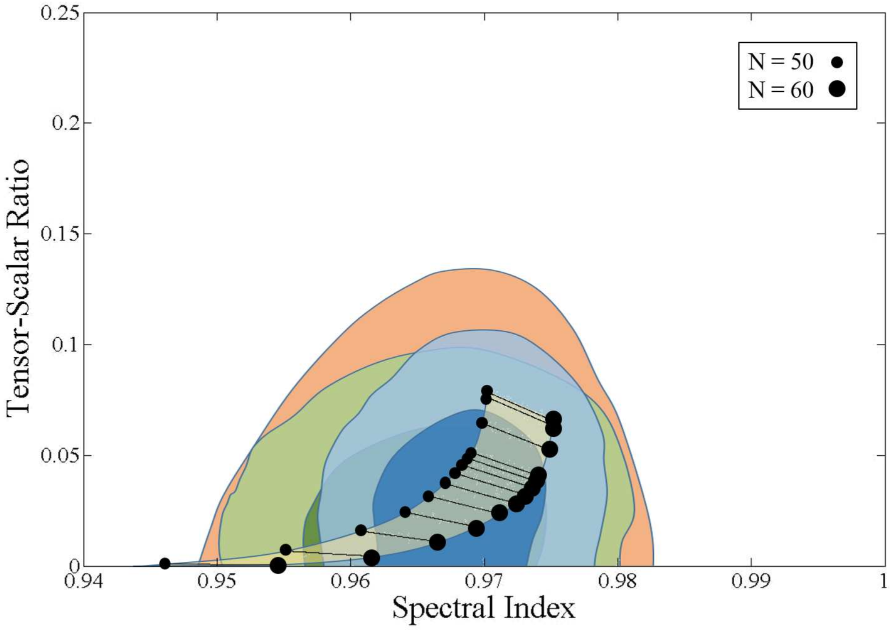

Figure 3.2: Plot of tensor-scalar ratio against spectral index for the potential $V = (1/4)\lambda\,(\phi_0^4 - \phi^4)$. Each line corresponds to a different value of x_0, starting from 5 and increasing to 50 in factors of five, then the values one-hundred, five-hundred and two-thousand have been included to see where the lines tend towards. The confidence regions of 68% and 95% from the Planck data have been superimposed. The labelling of the points where N is equal to fifty and sixty has been given in the top right of the plot.

```
    ylim([0 0.1])
    xlabel('Spectral Index')
    ylabel('Tensor-Scalar Ratio')
    hold on
end
```

which finds two-hundred-and-fifty different points, and after running, outputs the effect of a singular line on a plot such as the one in the worked example.

It is possible to take this one step further and return multiple lines on the same plot. However there is a problem with this. Each individual x_0 requires values for $x_\star$ when N is equal to fifty and sixty. As this is quite complex to do in a for loop, it is best to find all the values of $x_\star$ for different x_0 by hand by running the code, and then copy and pasting the entire script into a separate file multiple times, inputting the different values. This results in a MATLAB script which is over three hundred lines long for thirteen different values of x_0 yet only four different values (the x_0, two values for $x_\star$ and one two-hundredth of the difference between the two $x_\star$ values) need to be changed for each different value of x_0, making the code more effective than it seems.

Figure 3.2 shows the resultant plot when the values for x_0 range from five to fifty in multiples of five, and then the values one hundred, five hundred and two thousand to see where the lines are tending towards. The graphs have been edited to incorporate the Planck data for a direct comparison, and to show explicitly the values where N is equal to fifty and sixty for each different value of x_0.

A direct comparison with Figure 2.3 shows the trend towards a linear potential as x_0 gets larger, as expected from before.

When comparing the potential lines to the Planck data, the lines are full within the 95% confidence regions when x_0 is between twenty and fifty. Even with the higher values of x_0, the lines are fully within the 68% confidence regions. Therefore it can be deduced that this is a suitable potential when compared with the Planck data. However, there is a lack of experimental evidence that supports this model.

3.3 Soft SUSY

What about a more complicated model? With supersymmetry, a potential can be defined as

$$V \simeq \frac{1}{32\pi^2}\left[\sum_{i=1,2}\left(m_i^2+\frac{1}{2}\lambda\phi^2\right)^2-2\left(m_f^2+\frac{1}{2}\lambda\phi^2\right)^2\right]\ln\left(\frac{\phi}{Q}\right) \ ,$$

where m_1 and m_2 are masses for the real and imaginary part of a complex field, m_f is the mass of the field's fermionic partner and Q is the renormalization scale [16]. When m_i is equal to m_f, the result supersymmetry, and the potential collapses to equalling zero.

There are two breaking cases for this model. The first is when there is spontaneous SUSY breaking, which gives $2m_f^2 = m_1^2 + m_2^2$, and the resulting potential is

$$V \simeq \frac{\left(m_1^2-m_2^2\right)^2}{64\pi^2}\ln\left(\frac{\phi}{Q}\right) \ ,$$

as the coefficient of ϕ^2 disappears [16]. The other case is when there is soft

SUSY breaking, which is when m_f is equal to zero, resulting in

$$V \simeq \frac{1}{32\pi^2}\lambda\left(m_1^2+m_2^2\right)\phi^2\ln\left(\frac{\phi}{Q}\right) \ ,$$

as here the quadratic term overrides the others [16]. This is the basis for the soft SUSY model that will be investigated here, by rescaling λ so the potential becomes

$$V = \frac{1}{2}\lambda\phi^2\left(\ln\left(\frac{\phi^2}{\phi_0^2}\right)-1\right)+\frac{1}{2}\lambda\phi_0^2 \ , \tag{3.6}$$

which is a simpler potential to work with in MATLAB.

As before, it is best to rescale the potential in terms of x. Using the substitution $x = \phi/\phi_0$ results in the potential becoming

$$V = \frac{1}{2}x^2\left(\ln\left(x^2\right)-1\right)+\frac{1}{2} \ . \tag{3.7}$$

This scaling is different to before, which effects the MATLAB code, as will be shown later,

The derivative and the double derivative of the potential is needed. Differentiating equation (3.7) yields

$$V' = x\ln\left(x^2\right) \ , \tag{3.8}$$

and in turn, differentiating equation (3.8) results in

$$V'' = 2+\ln\left(x^2\right) \ . \tag{3.9}$$

These equations are defined in MATLAB using the following code

```
x0 = 10.0;
v = @(x) 0.5*x.*x.*(log(x.*x)-1.0) + 0.5;
dv = @(x) x.*log(x.*x);
d2v = @(x) 2 + log(x.*x);
eps = @(x) (0.5*((dv(x)).^2)./((v(x)).^2))/(x0.*x0);
eta = @(x) ((d2v(x))./v(x))/(x0.*x0);
```

where the x_0^{-2} terms in the ϵ and η are due to the choice of substitution.

As before, the potential can be plotted using the code

```
x = 1.0e-6:0.01:1-1.0e-6;
y = v(x);
figure
plot(x,y)
```

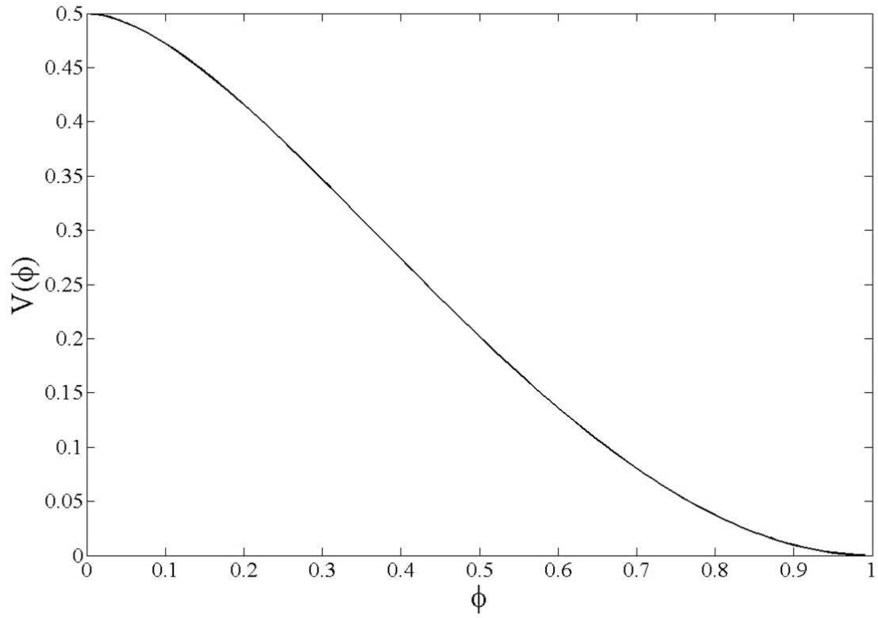

Figure 3.3: Graph of $V(\phi)$ against ϕ for the soft SUSY model. Here, x_0 has been taken to be ten.

where the range has changed from x_0 in the earlier potential to one in this potential, which is also due to substitution. This plot, seen in Figure 3.3, also shows that using the slow-roll approximation is suitable as the potential slowly rolls to a minimum, as before.

The only differences to the code in the earlier section and this code is the scaling with the x_0^{-2} terms, i.e. the x_r is now

```
xr = [1.0e-6,1.0-1.0e-6];
```

and the e-foldings term is now

```
efolds = @(x) (x0.*x0).*(v(x)./dv(x))
```

otherwise, the code carries on the same. Next is to find the values for when N is 50 and 60 when x_0 is equal to 10. By using trial and error, N is roughly found to be equal to 50 when $x_\star$ is equal to 0.003188, and N is roughly found to be equal to 60 when $x_\star$ is equal to 0.0001886, with both values for $x_\star$ given to four significant figures.

This trial and error method can be performed multiple times, as before. Figure 3.4 shows a plot of the soft SUSY model for smaller values of x_0; these values are the values between ten and twelve in factors of 0.2, and then the

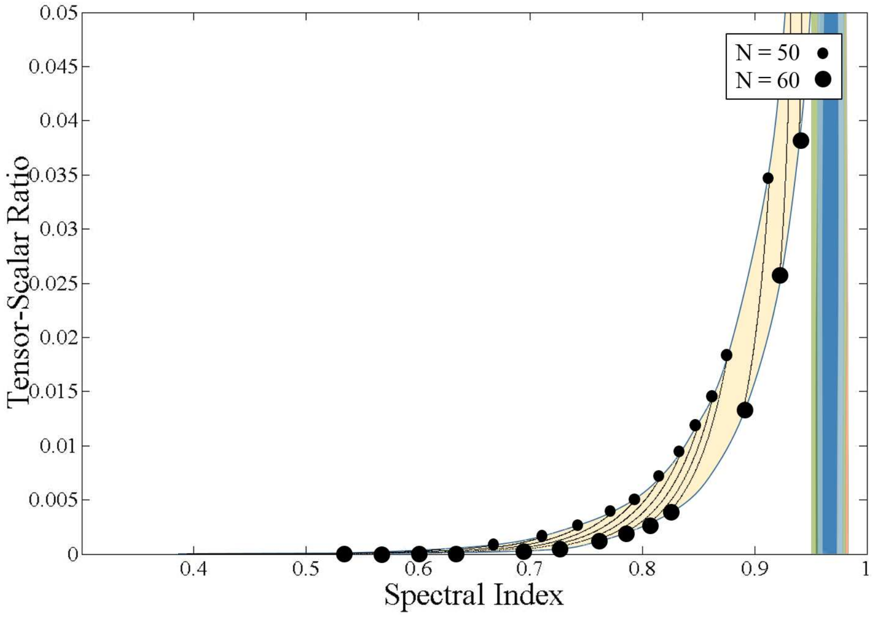

Figure 3.4: Plot of tensor-scalar ratio against spectral index for the soft SUSY model for small values of x_0, starting at ten and increasing in factors of 0.2 until twelve, then the plots for thirteen, fourteen and fifteen have been included to see where the lines are tending towards.

integers up to fifteen, as beyond this the lines are no longer on the plot due to the axes limits. This graph is different to what has been seen before as the lines have taken on a different shape, and by looking at the axes, it is clear to see that it has a completely different range of values for the tensor-scalar ratio and power spectrum. These plots for the lower values of x_0 are also nowhere near the Planck data. However, as x_0 gets larger, the lines seem to tend towards the Planck 68% and 95% confidence intervals. Therefore, it seem intuitive to look at the larger values of x_0 and then comparing graphs.

Figure 3.5 shows the resultant plot using the values for x_0 as the integers from ten to twenty, and also the values from twenty to fifty in multiples of five, however the spectral index axis has been limited to only plot between the values of 0.9 and 1, so any lines to the left of 0.9 are not shown in this figure.

As before, the graphs have been edited to incorporate the Planck data for a direct comparison, and to show explicitly the values where N is equal to fifty and sixty for each different value of x_0.

With small x_0, the logarithm part of the expression dominates, and this

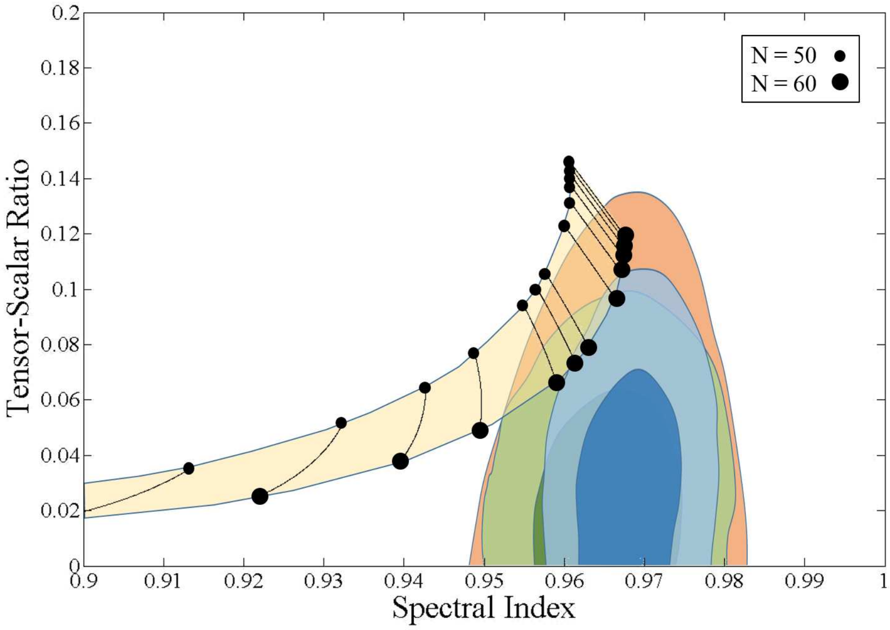

Figure 3.5: Plot of tensor-scalar ratio against spectral index for the soft SUSY model. Each line corresponds to a different value of x_0, starting from the integers between ten and twenty, then the values from twenty to fifty in factors of five have been included to see where the lines tend towards. The confidence regions of 68% and 95% from the Planck data have been superimposed. The labelling of the points where N is equal to fifty and sixty has been given in the top right of the plot.

is where the plot acts strangely. It is possible to see the evolution of the lines curving round and transforming into the straight lines of the potentials seen so far as the x_0 gets larger. In fact, a direct comparison with Figure 2.3 shows the trend towards a ϕ^2 potential as x_0 gets larger, as expected from the earlier assumptions, due to the $(1/2)\lambda\phi_0^2$ dominating. This would imply that larger values of x_0 are needed so that the model complies with the Planck data.

When comparing with the earlier Planck data, it is only when x_0 becomes larger than seventeen when the lines enter the 68% confidence regions, and none of the lines enter the 95% confidence regions. Due to this it can be deduced that this is not the best model to use, although it can be argued that when x_0 is between twenty and twenty-five, the majority of the line is within the 68% confidence region, so ideally using these values might be acceptable to use when modelling. Despite this, the soft SUSY model has experimental data on its side, whereas the $V = (1/4)\lambda\,(\phi_0^4 - \phi^4)$ model (which seems like the better model to use as it is fully within the confidence regions) does not. Therefore it might be preferable to use the soft SUSY model after all.

Chapter 4

Summary

To summarise, it has been shown that gravitational waves are an important field in modern cosmology. Found in the CMB, the fact that they exclusively polarise into B-modes makes it possible to detect. However, this is harder than at first thought. It is possible to get these signals confused with cosmic dust, as experienced by the BICEP2 collaboration. However the joint work done by the BICEP2 and Planck teams produced the most accurate description of the characteristics of the gravitational waves, hopefully meaning detection is not too far away. This detection would result in the first batch of clear experimental evidence for the theory of inflation and the big bang.

Inflation is a key part of gravitational wave analysis, as the power spectrum for the tensor incorporates the mean square of the gravitational wave amplitude. This has made it possible to plot the ratio of the gravitational wave amplitude and the density fluctuations against the spectral index. Inflation allows the use of different potential energy equations, meaning an almost endless amount of possibilities as to which can be modelled. However, experimental data can rule out most potentials after direct comparisons with confidence regions on the plots.

The use of MATLAB has paved the way for even more potential energy equations to be considered. The integral for the number of e-folding's proves a difficulty when trying to solve more difficult potentials by hand, however due to MATLAB's powerful problem solving ability, this no longer becomes a problem. Using this method, it has been shown that a potential of

$$V = \frac{1}{4}\lambda\left(\phi_0^4 - \phi^4\right) \ ,$$

is suitable to use when considered with the Planck data, yet has a lack of experimental evidence, and a soft SUSY potential, given by

$$V = \frac{1}{2}\lambda\phi^2\left(\ln\left(\frac{\phi^2}{\phi_0^2}\right) - 1\right) + \frac{1}{2}\lambda\phi_0^2 \ ,$$

does not lie within the confidence regions as fully as desired, yet it can be argued to be a suitable model as it does have experimental data on its side.

As elusive as finding them seems to be, scientists are on the cusp of detecting these primordial gravitational waves, which could possibly result in the discovery of the initial conditions for the origin of the universe, and hopefully an answer to the age old question of 'how did we get here?'.

Appendix A

Derivations

This section provides derivations of equations that were too large to fit into the main text.

A.1 Derivation of E-folds Equation

Starting with the equation for the number of e-folding's given earlier as

$$N = \ln\left(\frac{a\left(t_f\right)}{a\left(t_\star\right)}\right) \ .$$

Using laws of differentiating log functions, the equation above can be expressed as

$$N = \int_{a(t_\star)}^{a\left(t_f\right)} \frac{da}{a} \ ,$$

which can also be written as

$$N = \int_{\phi_\star}^{\phi_f} \frac{1}{a}\frac{da}{dt}\frac{dt}{d\phi}d\phi \ .$$

By using dots above parameters to denote time derivatives, and equation (2.4) for H the above equation can be expressed as

$$N = \int_{\phi_\star}^{\phi_f} H\frac{d\phi}{\dot{\phi}} \ .$$

This equation can be rewritten by using equation (2.11) to give

$$N = -\int_{\phi_\star}^{\phi_f} 3H^2\frac{d\phi}{V_\phi} \ ,$$

where $V_\phi = dV/d\phi$. To get the final expression, equation (2.10) can be substituted into the above equation, and constants can be taken outside of the integral to give

$$N = -8\pi G \int_{\phi_\star}^{\phi_f} \frac{V}{V_\phi} d\phi \ ,$$

as required.

A.2 Derivation of Tensor-Scalar Ratio

The equation for the tensor-scalar ratio was given earlier as

$$r = \frac{\mathcal{P}_T}{\mathcal{P}_S} \ .$$

The expressions for $\mathcal{P}_S$ and $\mathcal{P}_T$ from equations (2.17) and (2.18) respectively, can be substituted into the above to give

$$r = \frac{2}{\pi^2}\frac{H^2}{M_p^2}\left(\frac{1}{4\pi^2}\frac{H^4}{\dot{\phi}^2}\right)^{-1} \ .$$

Cancelling down terms in the above equation results in

$$r = \frac{8\dot{\phi}^2}{H^2 M_p^2} \ .$$

Using equation (2.11) in the expression above yields

$$r = \frac{8V_\phi^2}{H^2\left(9H^2\right)M_p^2} \ .$$

The denominator can be simplified, resulting in

$$r = \frac{8V_\phi^2}{\left(3H^2\right)^2 M_p^2} \ .$$

Inserting equation (2.10) into the above returns

$$r = \frac{8V_\phi^2}{\left(8\pi G V\right)^2 M_p^2} \ .$$

After cancelling through the M_p^2, the above equation and equation (2.12) can be compared to show that

$$r = 16\epsilon \ ,$$

as required.

A.3 Derivation of Spectral Index

Starting with the equation for the power spectrum for the scalar including n_S, the spectral index, given earlier as

$$\mathcal{P}_S \approx Ak^{n_S - 1} \ .$$

By taking logs and rearranging, the above equation transforms into

$$n_s = 1 + \frac{d \ln \mathcal{P}_S}{d \ln k} \ .$$

At the horizon crossing

$$k = a\left(t_k\right) H\left(t_k\right) \ ,$$

therefore it is correct to state that

$$\ln\left(k\right) = ln\left(a\right) + ln\left(H\right) \ .$$

It is also valid to say that

$$\frac{d \ln \mathcal{P}_S}{d \ln k} = \frac{d \ln \mathcal{P}_S}{dt_k} \left(\frac{d \ln k}{dt_k}\right)^{-1} \ .$$

Therefore the numerator and denominator can be evaluated independently as two different derivative expressions. Both of these expressions can be divided by H, as it makes evaluating the two statements simpler, and when put back into the fraction, get cancelled out anyway. Therefore the expression for the numerator gives

$$\frac{1}{H}\frac{d \ln \mathcal{P}_S}{dt_k} = \frac{4\dot{H}}{H^2} - \frac{2\ddot{\phi}}{H\dot{\phi}} \ .$$

Using equations (2.14) and (2.15) in the above expression gives the value for the numerator in terms of slow roll parameters as

$$\frac{1}{H}\frac{d \ln \mathcal{P}_S}{dt_k} = -4\epsilon - 2\left(\epsilon - \eta\right) \ .$$

By expanding out brackets and cancelling out in the above equation, the value of the numerator is expressed as

$$\frac{1}{H}\frac{d \ln \mathcal{P}_S}{dt_k} = 2\eta - 6\epsilon \ .$$

Using the same method, the expression for the denominator gives

$$\frac{1}{H}\frac{d \ln k}{dt_k} = \frac{1}{H}\left(\frac{\dot{a}}{a} + \frac{\dot{H}}{H}\right) \ .$$

Multiplying out the bracket results in

$$\frac{1}{H}\frac{d\ln k}{dt_k} = 1 + \frac{\dot{H}}{H^2} \ .$$

Using equation (2.15) in the above expression gives the value for the denominator in terms of slow roll parameters as

$$\frac{1}{H}\frac{d\ln k}{dt_k} = 1 - \epsilon \ .$$

Substituting these values into the fraction obtained in the equation for spectral index gives

$$n_s = 1 + \frac{2\eta - 6\epsilon}{1 - \epsilon} \ .$$

This can be simplified to give

$$n_s = 1 + 2\eta - 6\epsilon + \mathcal{O}\left(\epsilon\right) \ ,$$

as required.

Appendix B

MATLAB Code

This section provides the MATLAB code created to produce the graphs seen in the text, and the numerical values necessary of calculating solutions for complicated potentials.

B.1 Worked Example Graph Code

```
x=[0.942,0.951];
y=[0.314,0.262];
plot(x,y,'k','linewidth',2)
xlim([0.9 1]);
ylim([0 0.5]);
xlabel('Spectral Index')
ylabel('Tensor-Scalar Ratio')
```

B.2 Potential Involving ϕ^4 Code

```
%defining parameters and equations
xp = 10.0;
v = @(x) 1 - (x.^4)/(xp.^4);
dv = @(x)  -4*(x.^3)/(xp.^4);
d2v = @(x)  -12*(x.^2)/(xp.^4);
eps = @(x) 0.5*((dv(x)).^2)./((v(x)).^2);
eta = @(x) d2v(x)./v(x);

%plot
x = 1.0e-6:0.01:xp-1.0e-6;
y = v(x);
```

```
figure
plot(x,y,'k','linewidth',2)
xlabel('\phi')
ylabel('V(\phi)')

%epsilon = 1
eps1 = @(x) eps(x)-1.0;
xr = [1.0e-6,xp-1.0e-6];
xf = fzero(eps1,xr);

%integral
xstar = 4.136;
efolds = @(x) (v(x)./dv(x));
N = -integral(efolds,xstar,xf)

%N is roughly 50 when xstar = 4.136 to 4 s.f.
%N is roughly 60 when xstar = 3.873 to 4 s.f.

%to create plots
for i = 3.8728:0.0010516:4.1357
    xstar = i;
    r = 16.*eps(xstar);
    n = 1 + 2*eta(xstar) - 6*eps(xstar);
    plot(n,r,'k')
    xlim([0.94 1])
    ylim([0 0.1])
    xlabel('Spectral Index')
    ylabel('Tensor-Scalar Ratio')
    hold on
end
```

B.3 Soft SUSY Code

```
%defining parameters and equations
x0 = 10.0;
v = @(x) 0.5*x.*x.*(log(x.*x)-1.0) + 0.5;
dv = @(x) x.*log(x.*x);
d2v = @(x) 2 + log(x.*x);
eps = @(x) (0.5*((dv(x)).^2)./((v(x)).^2))/(x0.*x0);
eta = @(x) ((d2v(x))./v(x))/(x0.*x0);
```

```
%plot
x = 1.0e-6:0.01:1-1.0e-6;
y = v(x);
figure
plot(x,y,'k','linewidth',2)
xlabel('\phi')
ylabel('V(\phi)')

%epsilon = 1
eps1 = @(x) eps(x)-1.0;
xr = [1.0e-6,1.0-1.0e-6];
xf = fzero(eps1,xr);

%integral
xstar = 0.0001886;
efolds = @(x) (x0.*x0).*(v(x)./dv(x));
N = -integral(efolds,xstar,xf)

%N is roughly 50 when xstar = 0.003188 to 4 s.f.
%N is roughly 60 when xstar = 0.0001886 to 4 s.f.

%to create plots
for i = 0.0001886:0.000029994:0.003188
    xstar = i;
    r = 16.*eps(xstar);
    n = 1 + 2*eta(xstar) - 6*eps(xstar);
    plot(n,r,'k',)
    xlim([0 1]);
    ylim([0 0.0005]);
    xlabel('Spectral Index')
    ylabel('Tensor-Scalar Ratio')
    hold on
end
```

Bibliography

[1] Albert Einstein. Nherungsweise integration der feldgleichungen der gravitation. *Sitzungsberichte der Kniglich Preussischen Akademie der Wissenschaften Berlin*, 1916.

[2] University of Cambridge's Institute of Astronomy Website. *http://www.ast.cam.ac.uk/research/cosmology.and.fundamental.physics.*

[3] Andrei G. Doroshkevich, Igor D. Novikov, and Alexander G. Polnarev. Temperature fluctuations in the primordial background radiation due to gravitational waves. *Soviet Astronomy, volume 21*, 1977.

[4] Arno A. Penzias and Robert W. Wilson. A measurement of excess antenna temperature at 4080 mc/s. *Astrophysical Journal, volume 142*, 1965.

[5] European Space Agency Website. The planck satellite, space in images: Plnack power spectrum, space in images: Simulations of observations of the cmb. *http://www.esa.int/Our_Activities/Space_Science/Planck, http://www.esa.int/spaceinimages/Images/2013/03/Planck_Power_Spectrum, http://www.esa.int/spaceinimages/Images/2009/03/Simulations_of_observations_of_the_CMB.*

[6] National Aeronautics and Space Administration (NASA) Website. Wilkinson microwave anisotropy probe. *http://map.gsfc.nasa.gov/.*

[7] Wayne Hu. Intermediate guide to the acoustic peaks and polarization. *http://background.uchicago.edu/∼whu/intermediate/intermediate.html.*

[8] Peter A. Ade et al. (BICEP2 Collaberation). Bicep2 i: Detection of b-mode polarization at degree angular scales. *arXiv:1403.3985*, 2014.

[9] Peter A. Ade et al. (Planck Collaboration). Planck intermediate results. xxx. the angular power spectrum of polarized dust emission at intermediate and high galactic latitudes. *arXiv:1409.5738*, 2014.

[10] Alan H. Guth. Inflationary universe: A possible solution to the horizon and flatness problems. *Phys. Rev. D, volume 23*, 1981.

[11] Andrew R. Liddle. An introduction to cosmological inflation. *arXiv:astro-ph/9901124*, 1999.

[12] Andrew R. Liddle and David H. Lyth. Inflation and mixed dark matter models. *arXiv:astro-ph/9304017*, 1993.

[13] Peter A. Ade et al. (Planck Collaboration). Planck 2013 results. xxii. constraints on inflation. *arXiv:1303.5082*, 2013.

[14] William H. Kinney. Cosmology, inflation, and the physics of nothing. *arXiv:astro-ph/0301448*, 2004.

[15] Peter A. Ade et al. (Planck Collaboration). Planck 2015 results. xiii. cosmological parameters. *arXiv:1502.01589*, 2015.

[16] David H. Lyth and Antonio Riotto. Particle physics models of inflation and the cosmological density perturbation. *arXiv:hep-ph/9807278*, 1999.